

Damping modification factor based on random vibration theory using a source-based ground-motion model

Haizhong Zhang, Yan-gang Zhao^{*}

Department of Architecture, Kanagawa University, Yokohama, Japan

ARTICLE INFO

Keywords:

Damping modification factor
Random vibration theory
Source-based Fourier amplitude spectrum

ABSTRACT

Damping modification factor (DMF) plays an important role in seismic design and hazard analysis. Many studies have dedicated to the DMF, but the existing formulations still show a quite large scatter. This study proposes a new theoretical approach for analyzing the DMF. The proposed approach models the seismic ground motion with a source-based Fourier amplitude spectrum (FAS) and estimates the DMF from the FAS based on random vibration theory. Using the proposed approach, the characteristics of the DMF are explored and explained. It is found that trends in the DMF with variation of the structural period and seismological parameters are mainly controlled by the shape of the FAS. The overall shapes of the DMF and FAS are almost symmetrical with respect to the period axis. When the shape of the FAS changes with seismological parameters, the DMF changes accordingly, and their shapes nearly always remain symmetrical.

1. Introduction

In both seismic design and hazard analysis, the response spectral values are typically specified corresponding to only a 5% damping ratio. In reality, the damping ratio of a structural system depends on its characteristics and is not always 5%. For example, structures with isolation systems [1] or energy dissipation devices [2] typically have damping ratios much greater than 5%. It is therefore often necessary to adjust the spectral values at a 5% damping ratio to other required damping levels. At present, the most effective way to solve this problem is using the damping modification factor (DMF).

Since the 1980s, numerous studies have been conducted that focused on the DMF. The results from some early studies have been incorporated into seismic codes. Newmark and Hall [3] proposed three widely known formulas that are valid in the constant-acceleration, constant-velocity, and constant-displacement spectral regions. Parts of these formulas were adopted into the Uniform Building Code (UBC) [4] and the International Building Code (IBC) [5] for the design of structures with isolation systems or passive energy dissipation devices. Kawashima and Aizawa [6] proposed a formula for absolute spectral acceleration using 206 strong-motion records obtained at free-field stations in Japan. Their formulation was implemented in the Caltrans Seismic Design Criteria [7]. Ashour developed a formula for spectral displacement based on three recorded and 12 artificial earthquake accelerograms [8], which

was implemented in an early version of the UBC [9]. Similarly, another equation developed by Bommer and Elnashai [10] using a large dataset of European strong-motion records was adopted by Eurocode 8 [11]. A revision of this formula was subsequently suggested by Tolis and Faccioli [12], using the records of the 1995 Kobe earthquake. In addition, a trilinear model by Ramirez et al. [13] that considered ten strong motion records was implemented in the current National Earthquake Hazards Reduction Program (NEHRP) for Recommended Seismic Provisions for New Buildings [14]. Most of the formulas for the DMF that have been incorporated into seismic codes are mainly considered as functions of damping ratio alone.

Lin and Chang [15] pointed out that the DMF varies significantly with the structural period, particularly for higher damping ratios and longer periods, by analyzing 1053 accelerograms from 102 earthquakes in USA. Some studies further pointed out that the DMF depends not only on the structural parameters, i.e., structural period and damping ratio, but also on the seismological parameters, e.g., magnitude, site-to-source distance, and local site conditions. Lin and Chang [16] also investigated the effects of site conditions on the DMF using a database of 1,037 records classified on the basis of the different soil conditions defined in the NEHRP 2000 Provisions [14]. Bommer and Mendis [17] further explored the effects of three seismological parameters, including magnitude, site-to-source distance, and site conditions, based on three empirical ground-motion prediction equations for response spectra and

^{*} Corresponding author.

E-mail address: zhao@kanagawa-u.ac.jp (Y.-g. Zhao).

stochastic simulations. Cameron and Green [18], Hao et al. [19], and Rezaeian et al. [20] studied the effects of the three seismological parameters using a large number of actual strong-motion records. In addition, some studies [21–23] have investigated the effects of the duration of ground motion and the number of cycles on the DMF. Other studies [24–28] discussed the DMF of pulse-like ground motion based on a large number of near-fault strong-motion records. Hatzigeorgiou [24] also examined the effects of 100 artificial earthquakes on the DMF. Xiang et al. [29] studied the effects of the seismological parameters on the DMF of the vertical seismic motions. These studies developed many formulations for the DMF considering the structural period and various seismological parameters.

However, nearly all of the aforementioned studies are based on statistical analysis of recorded or artificial earthquake accelerograms. Since such statistical analysis is sensitive to the particular seismic data that is used, formulations based on different data sets still show a large scatter [30,31]. In addition, the statistical literature has yet to elucidate a clear understanding of the observed trends [30,31]. Recently, several theoretical approaches have been developed. Palermo et al. [30] derived an expression for the DMF by modeling the surface ground motion with the Kanai–Tajimi power spectral density and measuring the response spectral amplitude by the standard deviation of the displacement response. Greco et al. [31–33] developed another approach for determination of the DMF by modeling the surface ground motion with a non-stationary stochastic process developed by Clough and Penzien [34]. Clough and Penzien generated ground motion by modulating a stationary Gaussian white noise process by passing it through two linear filters. These theoretical approaches allow to the exploration and explanation of the effects of the structural parameters and site conditions on the DMF, which helps to reduce the scatter of the DMF formulas. However, it is still difficult to use these approaches to directly discuss the effects of some important seismological parameters, such as magnitude and site-to-source distance. Since the ground-motion models adopted in these studies are all site based, they do not explicitly incorporate these seismological parameters. Although the effects of the seismological parameters can be implicitly reflected to some extent by artificially adjusting parameters in the ground-motion model, such adjustments lack physical constraints and practical verification. To clearly understand the effects of the seismological parameters on the DMF, an approach using a source-based ground-motion model that explicitly includes the seismological parameters is desirable.

In this study, a new theoretical approach for analysis of the DMF is proposed. The ground motion is modeled using a source-based Fourier amplitude spectrum (FAS) that explicitly incorporates the seismological parameters. Since the FAS can be used to calculate the root-mean-square (RMS) value based on Parseval's theorem, and hence the peak value based on random vibration theory (RVT), it can also be used to obtain the response spectrum representing the peak values of the oscillator systems. Subsequently, an equation for the DMF can be obtained as the ratio of the response spectrum with a given damping ratio to that with a 5% damping ratio. Due to the use of a source-based ground-motion model and the simple equation for the DMF, trends in the DMF with variation of the seismological and structural parameters can be easily explored and explained.

The rest of the paper is organized as follows. Firstly, the proposed approach for analysis of the DMF is introduced in Section 2. The ground-motion model and RVT are introduced in Sections 2.1 and 2.2, respectively, and the equation for analysis of the DMF is derived using the FAS based on RVT, in Section 2.3. In Section 3, using the developed approach, trends in the DMF with variation of the structural and seismological parameters are explored and explained. Finally, the conclusions are presented in Section 4.

2. Proposed approach for analysis of the DMF

To theoretically explore and explain the effects of the seismological

Table 1
Parameters used in the development of the FAS.

| Parameter | Value |
|--|---|
| Stress drop $\Delta\sigma$ (bar) | 100 |
| Site diminution k (s) | 0.04 |
| Density of crust ρ (g/cm^3) | 2.8 |
| Shear-wave velocity of crust β (km/s) | 3.7 |
| Crust amplification $A(f)$ | Boor and Joyner [37] Generic Rock |
| Geometrical spreading $Z(R)$ | Atkinson and Boore [38] and Frankel et al. [39] |
| Path attenuation | $Q = 680f^{0.38}$ |

parameters on the DMF, which can hardly be examined using existing approaches, a new approach for analysis of the DMF is developed in this section. For this purpose, a source-based ground-motion model of the FAS that explicitly incorporates various seismological parameters is adopted. Since the FAS can be used to calculate the RMS value based on Parseval's theorem, and hence the peak value using a peak factor based on RVT, the response spectrum representing the peak values of the oscillator systems can then be obtained from the FAS. Subsequently, an equation for the DMF is obtained as the ratio of the response spectrum with a given damping ratio to that with a 5% damping ratio.

2.1. Earthquake ground-motion model

There are many approaches to obtaining the FAS, and one of the simplest is to compute it from a point source in terms of the various source, path, and site parameters using seismology theory. This study utilizes such a model using the point source spectrum described by Boore [34]. This ground-motion model has been well validated by comparison with observations from actual seismic records [35,36]. The FAS of acceleration ground motion at the surface, $Y(f)$, is expressed as an explicit function of the source term $E(M_0, f)$, the propagation path term, $P(R, f)$, and the site term, $G(f)$, such that

$$Y(f) = E(M_0, f)P(R, f)G(f) \quad (1)$$

where, f is frequency, R is the site-to-source distance, and M_0 is the seismic moment. The seismic moment M_0 can be related to moment magnitude M by

$$M_0 = 10^{1.5M+16.05} \quad (2)$$

The source term $E(M_0, f)$ is commonly expressed by the Brune ω -squared point source spectrum, although many other source spectrum models are equally valid [35]. Substituting the ω -squared point source spectrum and the expressions for the path and site terms [35] into Eq. (1) results in

$$Y(f) = \left[0.78 \frac{\pi}{\rho\beta^3} M_0 \frac{f^2}{1 + (f/f_c)^2} \right] \left[Z(R) \cdot \exp\left(\frac{-\pi f R}{Q(f)\beta}\right) \right] \left[\exp(-\pi k f) A(f) \right] \quad (3)$$

where, ρ is the mass density of the crust, β is the shear-wave velocity of the crust, $Z(R)$ represents the geometric attenuation, $Q(f)$ represents the anelastic attenuation, k is the diminution parameter, $A(f)$ represents the crust amplification, and f_c is the corner frequency representing the frequency below which the FAS decays, which is defined as

$$f_c = 4.9 \bullet 10^6 \beta (\Delta\sigma/M_0)^{1/3} \quad (4)$$

where, $\Delta\sigma$ is the stress drop.

Typical values of the parameters required for Eqs. (3) and (4) are determined based on Boore [35] and are shown in Table 1. The values of these parameters may be different for different regions. As this paper focuses on exploring and explaining the characteristics of the DMF, the values in Table 1 are simply determined within a reasonable range. If one wants to analyze the DMF of a specific region, appropriate values for

the parameters should be chosen for this region.

2.2. Random vibration theory

To obtain the DMF from the FAS introduced above, RVT is applied. RVT was first used in seismology by Hanks and McGuire [40] to predict the peak value from the RMS value. Subsequently, the approach was extended in engineering seismology and site-response analysis to estimate the peak acceleration, response spectrum [35,36], and site response [41–45] from the FAS. This study further extends the approach to the computation of the DMF from the FAS. The key feature of RVT is that it can relate the peak acceleration of the time-domain motion to the FAS of the motion using a peak factor, which is expressed as

$$a_{\max} = pf \sqrt{\frac{1}{D\pi} \int_0^\infty |Y(\omega)|^2 d\omega} = pf \sqrt{\frac{m_0}{D}} \quad (5)$$

where, a_{\max} is the peak acceleration, pf is the peak factor, D is the duration, ω is circular frequency, and $Y(\omega)$ is the FAS of the motion. The square root term in Eq. (5) represents the RMS acceleration according to Parseval's theorem. The parameter m_0 is the zeroth-order spectral moment of the FAS, and the n th order spectral moment of the FAS, m_n , is defined by

$$m_n = \frac{1}{\pi} \int_0^\infty \omega^n |Y(\omega)|^2 d\omega \quad (6)$$

The peak factor pf is a random variable for a stochastic process, and the expected value \overline{pf} is commonly used in RVT analysis. Many models for \overline{pf} have been developed [46–48], among which that of Cartwright and Longuet-Higgins [46] is commonly used in engineering seismology and site-response applications. The Cartwright and Longuet-Higgins model was derived by assuming that the peaks of a signal are independent and follow a Poisson process, which is expressed as

$$\overline{pf} = \sqrt{2} \int_0^\infty \left\{ 1 - \left[1 - \zeta e^{-\eta^2} \right]^{N_e} \right\} d\eta \quad (7)$$

where, ζ is a parameter that measures the bandwidth of the FAS

$$\zeta = \frac{m_2}{\sqrt{m_0 m_4}} = \frac{N_z}{N_e} \quad (8)$$

Here, N_e represents the number of extrema, estimated by

$$N_e = 2f_c D = \frac{1}{\pi} \sqrt{\frac{m_4}{m_2}} D \quad (9)$$

N_z represents the number of zero crossings, estimated by

$$N_z = 2f_z D = \frac{1}{\pi} \sqrt{\frac{m_2}{m_0}} D \quad (10)$$

f_e represents the rate of extrema and f_z represents the rate of zero crossings. For large values of N_e , Eq. (7) can be simplified as

$$\overline{pf} = [2 \ln(N_e)]^{1/2} + \frac{0.5772}{[2 \ln(N_e)]^{1/2}} \quad (11)$$

Equation (11) provides a more convenient calculation for the peak factor while sacrificing some accuracy. For simplicity, Eq. (11) is used in this study.

In addition, it should be noted that the duration D should be varied depending on the estimation objectives. When the RVT is used to estimate the peak acceleration of the ground motion, D is taken as the duration of the ground motion D_{gm} ; when the RVT is applied to estimate the ground-motion response spectrum, D is taken as the duration of the oscillator response of the ground motion D_{rms} . Boore and Joyner [49] first proposed an equation for estimation of D_{rms} from D_{gm} , and Liu and Pezeshk [50] subsequently suggested a revision of this formula,

$$D_{rms} = D_{gm} + \frac{1}{\overline{\omega} \xi} \left(\frac{(\overline{\omega} D_{gm} / 2\pi)^3}{(\overline{\omega} D_{gm} / 2\pi)^3 + 1/3} \right) \quad (12)$$

Here, $\overline{\omega}$ is the oscillator circular frequency, and ξ is the oscillator damping ratio. The duration of the ground motion is determined by $D_{gm} = 1/f_c + 0.05R$ according to Atkinson and Silva [51]. And many, more accurate equations for D_{rms} have been recently proposed [52,53], Eq. (12) is used in this study because of its simplicity.

2.3. Equation for the DMF

According to the FAS and RVT introduced above, an equation for determining the DMF is derived in this section. As the response spectrum represents the peak value of the oscillator response, according to Eq. (5), the acceleration response spectrum $S(\overline{\omega}, \xi)$ for an oscillator circular frequency $\overline{\omega}$ and damping ratio ξ can be expressed as

$$S(\overline{\omega}, \xi) = \overline{pf}_\xi \sqrt{\frac{1}{D_{rms-\xi} \pi} \int_0^\infty |YR(\omega, \overline{\omega}, \xi)|^2 d\omega} \quad (13)$$

where, \overline{pf}_ξ and $D_{rms-\xi}$ are the peak factor and the duration, respectively, of the oscillator response of the ground motion. The term $YR(\omega, \overline{\omega}, \xi)$ is the FAS of the oscillator response,

$$YR(\omega, \overline{\omega}, \xi) = Y(\omega)H(\omega, \overline{\omega}, \xi) \quad (14)$$

Here, $H(\omega, \overline{\omega}, \xi)$ is the oscillator transfer function for the pseudo-acceleration response spectrum considered in this study, which is expressed as

$$H(\omega, \overline{\omega}, \xi) = \frac{1}{\sqrt{(2\xi\omega/\overline{\omega})^2 + ((\omega/\overline{\omega})^2 - 1)^2}} \quad (15)$$

The DMF can then be obtained as the ratio of the response spectrum $S(\overline{\omega}, \xi)$ with a given damping ratio ξ to the conventional 5%-damped response spectrum $S(\overline{\omega}, 5\%)$, such that

$$DMF(\overline{\omega}, \xi) = \sqrt{\frac{\int_0^\infty |YR(\omega, \overline{\omega}, \xi)|^2 d\omega}{\int_0^\infty |YR(\omega, \overline{\omega}, 5\%)|^2 d\omega}} \times \frac{\overline{pf}_\xi}{\overline{pf}_{5\%}} \times \frac{\sqrt{D_{rms-5\%}}}{\sqrt{D_{rms-\xi}}} \quad (16)$$

where, $\overline{pf}_{5\%}$, $D_{rms-5\%}$, and $YR(\omega, \overline{\omega}, 5\%)$ represent the peak factor, duration, and the FAS, respectively, of the oscillator response corresponding to a 5% damping ratio. Equation (16) provides an analytical expression for the DMF.

Equation (16) is the product of three terms: the first term is determined by the FAS of the oscillator response, the second term is determined by the peak factors of the oscillator response, and the third term is determined by the signal durations of the oscillator response. Physically, the three terms represent the change in the FAS, the peak factor, and the signal duration of the oscillator response due to variation of the damping ratio ξ , respectively. In addition, it should be noted that the oscillator period T_0 ($= 2\pi/\overline{\omega}$) and damping ratio ξ in Eq. (16) represent the structural period and damping ratio in structural seismic design, respectively. For clarity and simplicity, the oscillator period is used instead of the structural period, and the oscillator damping ratio or structural damping ratio is abbreviated to simply “damping ratio” in the following discussions.

3. Discussion of the DMF based on the proposed approach

In this section, the characteristics of the DMF are explored and explained based on Eq. (16). As introduced above, the expression for the DMF is composed of three terms: the FAS term, the peak-factor term, and the duration term. Before exploring the characteristics of the DMF, it is interesting to understand how each term contributes to the DMF. For

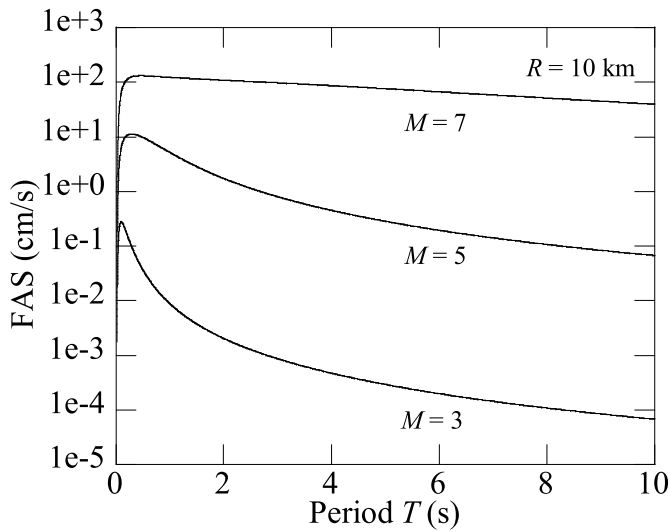


Fig. 1. Fourier amplitude spectra with $M = 3, 5,$ and $7,$ and $R = 10$ km.

this purpose, a series of FAS with $M = 3, 5,$ and $7,$ and $R = 10$ km, were generated using Eq. (3) and shown in Fig. 1. The DMF is then calculated considering a variety of damping ratios from 10 to 50%. Fig. 2 shows the calculated DMF results; Fig. 3 shows the corresponding values of the first term; and Figs. 4 and 5 show the corresponding values of the second and third terms, respectively.

By comparing the results in Figs. 2 and 3, it can be seen that the DMF is very similar to the first term for all the considered cases, including their values, shapes, and particularly the trends with variation of the oscillator period $T_0,$ damping ratio $\xi,$ and magnitude $M.$ Examination of Fig. 4 reveals that the values of the second term are very close to unity for all the cases considered. Fig. 5 indicates that, although the values of the third term are larger than unity for some periods, they are much closer to unity than those of the first term. These results imply that the first term significantly contributes to the DMF, and its contribution is much greater than the contributions of the second and third terms. Therefore, in the following discussions, the first term in Eq. (16) is used as a proxy for the DMF to explain its characteristics.

3.1. Dependence of the DMF on the oscillator period

The dependence of the DMF on the oscillator period is discussed in this section. It can be seen from Fig. 2 that the trend in the DMF with variation of the oscillator period T_0 is typically consistent with that observed from statistical analysis of recorded seismic motions [15,19], which provides an additional verification of the proposed approach. The value of the DMF is unity at an oscillator period of zero, and it then decreases with increasing oscillator period. When the oscillator period reaches a certain value, the DMF value becomes a minimum. The value of the DMF then starts to increase with the oscillator period, but the value never exceeds unity. By comparing Figs. 1 and 2, it can be seen that the trend in the DMF with variation of the oscillator period T_0 is opposite to that in the FAS with variation of its period $T,$ and the overall shapes of the DMF and FAS are nearly symmetrical with respect to the

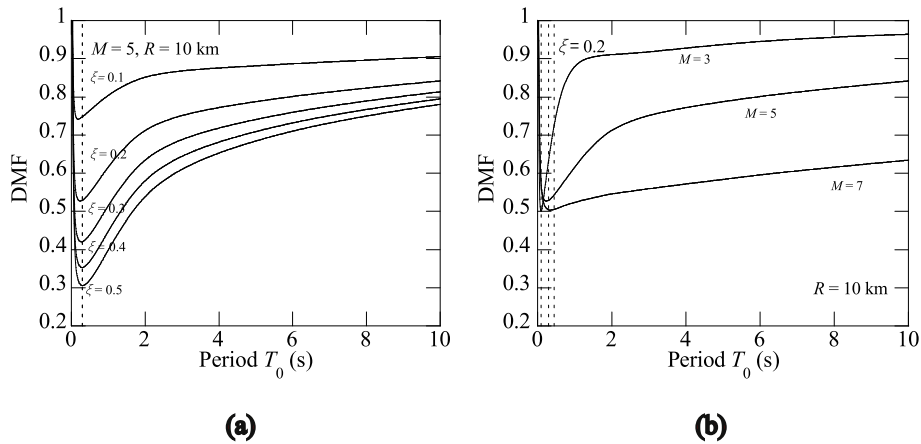


Fig. 2. Values of the DMF with: (a) ξ varying from 0.1 to 0.5; (b) M varying from 3 to 7.

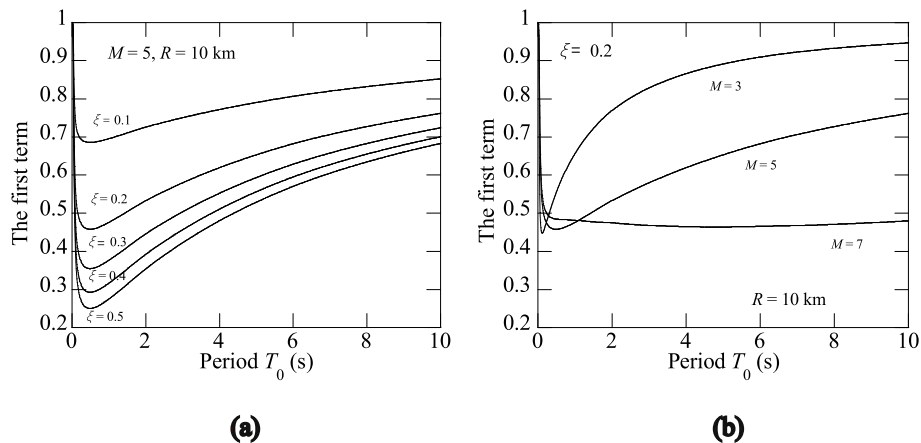


Fig. 3. Values of the first term with: (a) ξ varying from 0.1 to 0.5; (b) M varying from 3 to 7.

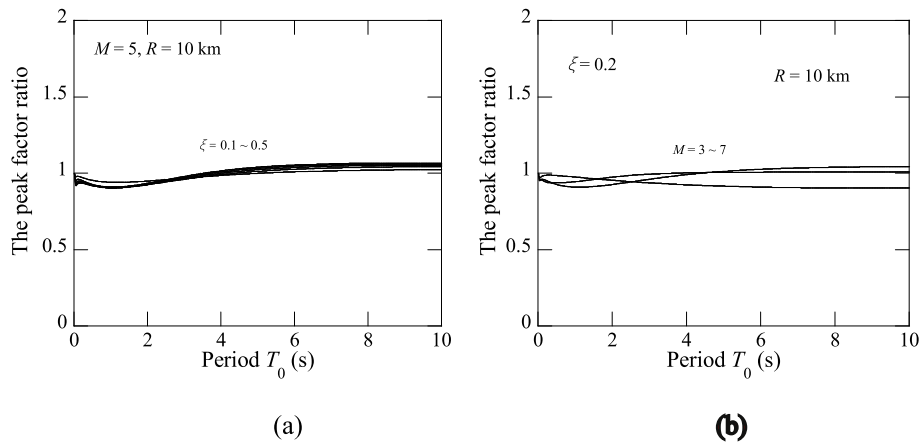


Fig. 4. Values of the second term, i.e., the peak factor ratio $\overline{pf}_\xi / \overline{pf}_{5\%}$ with: (a) ξ varying from 0.1 to 0.5; (b) M varying from 3 to 7.

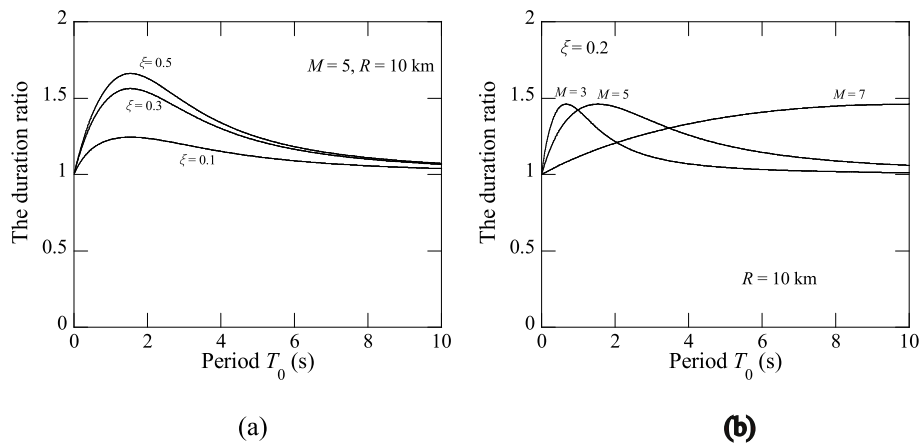


Fig. 5. Values of the third term, i.e., the duration ratio $\sqrt{D_{rms*5\%} / D_{rms*\xi}}$ with: (a) ξ varying from 0.1 to 0.5; (b) M varying from 3 to 7.

period axis. The minimum value of the DMF almost coincides with the peak of the FAS. The period at which the peak of the FAS occurs is represented by dotted line in Fig. 2. Here, it should be noted that the period of the FAS T is physically different from the oscillator period T_0 .

To explain the trend in the DMF with variation of the oscillator period, the first term of Eq. (16) is analyzed in detail. The first term equals the ratio of $\sqrt{\int_0^\infty |YR(\omega, \bar{\omega}, \xi)|^2 d\omega}$ to $\sqrt{\int_0^\infty |YR(\omega, \bar{\omega}, 5\%)|^2 d\omega}$. According to Eq. (6), $\int_0^\infty |YR(\omega, \bar{\omega}, \xi)|^2 d\omega$ is the zeroth-order spectral moment of the acceleration response, and $|YR(\omega, \bar{\omega}, \xi)|^2$ acts as the zeroth-moment integrand. The zeroth-order spectral moment mathematically represents the area enclosed by $|YR(\omega, \bar{\omega}, \xi)|^2$ with the frequency axis. Therefore, the DMF can be regarded as a measure of the

change in the area of $|YR(\omega, \bar{\omega}, \xi)|^2$ with the damping ratio. When the area of $|YR(\omega, \bar{\omega}, \xi)|^2$ decreases relative to that of $|YR(\omega, \bar{\omega}, 5\%)|^2$, the DMF will decrease; conversely, when the area of $|YR(\omega, \bar{\omega}, \xi)|^2$ increases relative to that of $|YR(\omega, \bar{\omega}, 5\%)|^2$, the DMF will increase.

To understand the characteristics of the area of $|YR(\omega, \bar{\omega}, \xi)|^2$, the behavior of the zeroth-moment integrand $|YR(\omega, \bar{\omega}, \xi)|^2$ with variation of the damping ratio and oscillator period are investigated. For this purpose, values of $|YR(\omega, \bar{\omega}, \xi)|^2$ versus the period T for three representative oscillator periods, $T_0 = 0.03$ s, 0.3 s, and 8 s are shown in Fig. 6. The dotted line represents the results corresponding to a 5% damping ratio, and the solid line represents the results corresponding to a 30% damping ratio.

It is noted from Fig. 6 that with increasing damping ratio,

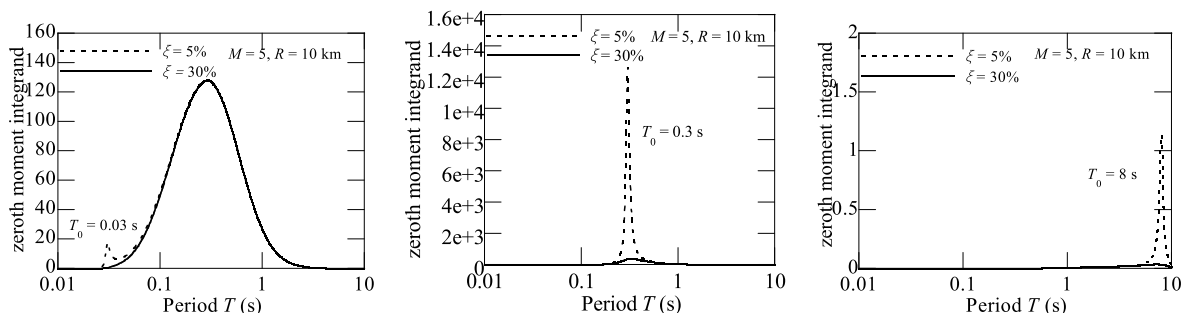


Fig. 6. Dependence of $|YR(\omega, \bar{\omega}, \xi)|^2$ on the damping ratio ξ and oscillator period T_0 .

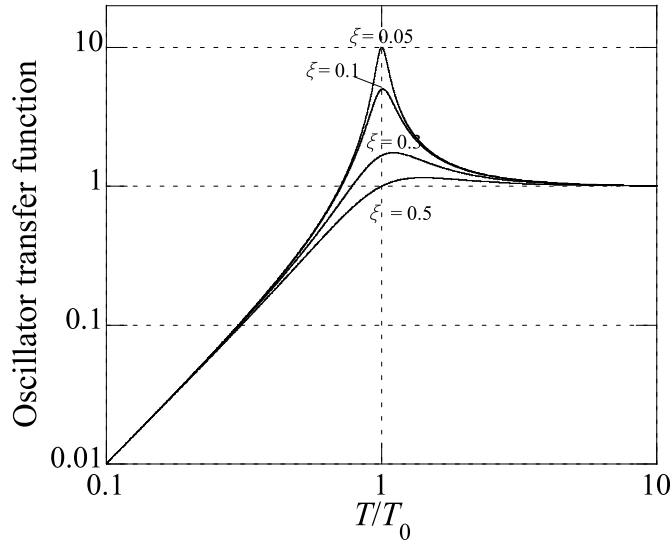


Fig. 7. Values of the oscillator transfer functions for various of damping ratios.

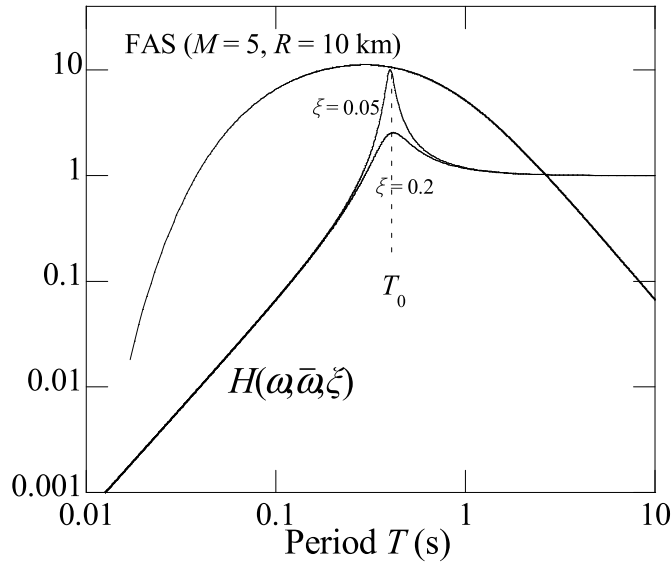


Fig. 8. Illustration of the calculation of the DMF.

$|YR(\omega, \bar{\omega}, \xi)|^2$ decreases mainly at periods around the oscillator period T_0 and is almost unaffected at other periods. In addition, the values of $|YR(\omega, \bar{\omega}, \xi)|^2$ near to T_0 are strongly dependent on the value of T_0 . When T_0 is very short (0.03 s), the values of $|YR(\omega, \bar{\omega}, \xi)|^2$ at periods around T_0 are very small; but when the oscillator period increases and approaches the period at which the peak of the FAS occurs (0.3 s), the values become very large; then, as T_0 increases further (8 s), the values decrease again.

Since $YR(\omega, \bar{\omega}, \xi)$ is the product of the ground-motion FAS and the oscillator transfer function $H(\omega, \bar{\omega}, \xi)$ (Eq. (14)), the behavior of $|YR(\omega, \bar{\omega}, \xi)|^2$ with variation of the damping ratio and oscillator period can be understood by further analyzing the FAS and $H(\omega, \bar{\omega}, \xi)$. It is noted that the oscillator transfer function $H(\omega, \bar{\omega}, \xi)$ varies with the damping ratio ξ but the FAS does not. Thus, the change in the values of $|YR(\omega, \bar{\omega}, \xi)|^2$ with the damping ratio is solely caused by variation of the oscillator transfer function. Fig. 7 shows values of the oscillator transfer function for a variety of damping ratios. It is found that the values of the oscillator transfer function decrease mainly at periods around the oscillator period T_0 , i.e., $T/T_0 \approx 1$, with increasing damping ratio. This explains why $|YR(\omega, \bar{\omega}, \xi)|^2$ decreases mainly at periods around the

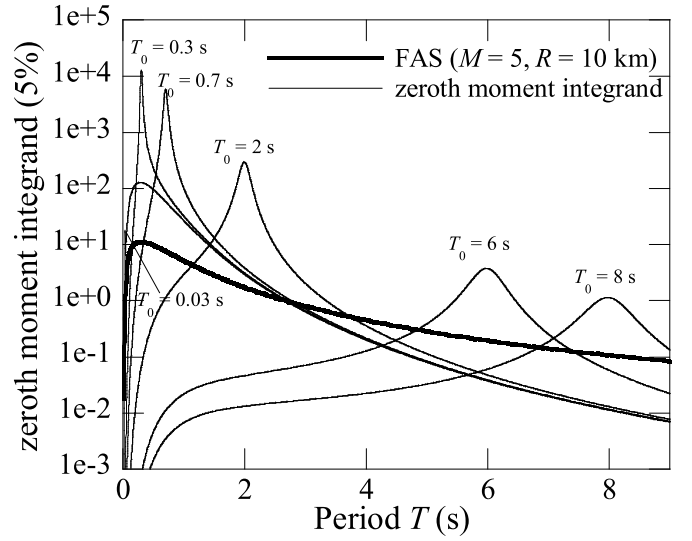


Fig. 9. Comparison of $|YR(\omega, \bar{\omega}, 5\%)|^2$ for oscillator periods from 0.03 to 8 s.

oscillator period with increasing damping ratio (Fig. 6). In addition, Fig. 7 and Eq. (15) indicate that the oscillator transfer function is a function of the period ratio T/T_0 , and its values at periods around the oscillator period, i.e., $T/T_0 \approx 1$, are constant for a specific damping ratio; thus, the variation of $|YR(\omega, \bar{\omega}, \xi)|^2$ at periods around T_0 with the value of T_0 is mainly due to the change of the FAS. As illustrated by Fig. 8, when the oscillator period T_0 is near zero where the FAS is very small, the values of $|YR(\omega, \bar{\omega}, \xi)|^2$ at periods around the oscillator period are small; but when the oscillator period is near the peak of the FAS, the values are very large. Then, as the oscillator period increases where the FAS decreases, the values also decrease. Values of $|YR(\omega, \bar{\omega}, \xi)|^2$ at periods around the oscillator period are proportional to those of the FAS at the same periods.

To better explain the trend in the DMF with variation of the oscillator period, the area of $|YR(\omega, \bar{\omega}, \xi)|^2$ is then divided into two parts: one represents the area around the oscillator period where $|YR(\omega, \bar{\omega}, \xi)|^2$ decreases with increasing damping ratio, expressed by $P_e(\bar{\omega}, \xi)$; the other represents the area where $|YR(\omega, \bar{\omega}, \xi)|^2$ remains almost constant with changing damping ratio, expressed by $S(\bar{\omega})$. Hence, the DMF can be approximately expressed as

$$DMF(\bar{\omega}, \xi) = \sqrt{\frac{S(\bar{\omega}) + P_e(\bar{\omega}, \xi)}{S(\bar{\omega}) + P_e(\bar{\omega}, 5\%)}} = \sqrt{\frac{S(\bar{\omega}) + r(\xi)P_e(\bar{\omega}, 5\%)}{S(\bar{\omega}) + P_e(\bar{\omega}, 5\%)}} \quad (17)$$

where, $r(\xi)$ ($r < 1$ for $\xi > 5\%$) represents the rate of reduction in the area of $|YR(\omega, \bar{\omega}, \xi)|^2$ around the oscillator period due to increasing damping ratio. As the change in the area of $|YR(\omega, \bar{\omega}, \xi)|^2$ with the damping ratio is solely due to the change in the oscillator transfer function, to investigate the rate of reduction in the area of $|YR(\omega, \bar{\omega}, \xi)|^2$, an expression representing the rate of reduction in the oscillator transfer function is obtained as

$$\frac{H(\omega, \bar{\omega}, \xi)}{H(\omega, \bar{\omega}, 5\%)} = \sqrt{\frac{(0.1\omega/\bar{\omega})^2 + ((\omega/\bar{\omega})^2 - 1)^2}{(2\xi\omega/\bar{\omega}) + ((\omega/\bar{\omega})^2 - 1)^2}} \quad (18)$$

Since Eq. (18) is also a function of the period ratio T/T_0 , the reduction rates at periods around the oscillator period, i.e., $T/T_0 \approx 1$, are constant for a specific damping ratio. Therefore, $r(\xi)$ is approximately considered to be independent of the oscillator period.

Equation (17) indicates that the value of the DMF is inversely proportional to the relative size of $P_e(\bar{\omega}, 5\%)$ with respect to $S(\bar{\omega})$, and that

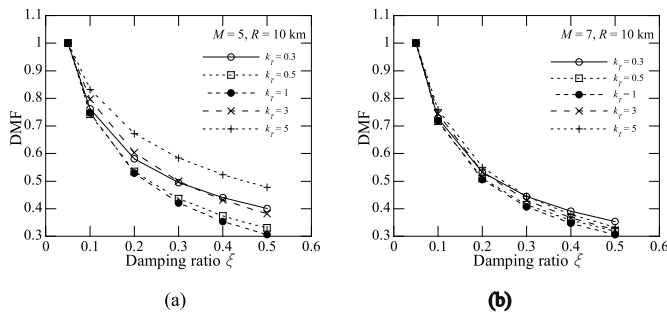


Fig. 10. Dependence of the DMF on the damping ratio ξ , with (a) $M = 5$, $R = 10$ km; (b) $M = 7$, $R = 10$ km.

the maximum and minimum values of the DMF equal unity and $\sqrt{r(\xi)}$, respectively. The larger $P_e(\bar{\omega}, 5\%)$ is with respect to $S(\bar{\omega})$, the closer the DMF is to the minimum value, i.e., $\sqrt{r(\xi)}$; conversely, the smaller $P_e(\bar{\omega}, 5\%)$ is with respect to $S(\bar{\omega})$, the closer the DMF is to the maximum value, i.e., unity. To investigate how $P_e(\bar{\omega}, 5\%)$ varies relative to $S(\bar{\omega})$ with the oscillator period, values of $|YR(\omega, \bar{\omega}, 5\%)|^2$ for a series of oscillator periods from 0.03 to 8 s are compared in Fig. 9. It is observed that the behavior of $P_e(\bar{\omega}, 5\%)$ relative to $S(\bar{\omega})$ with variation of the oscillator period is typically consistent with that of the values of $|YR(\omega, \bar{\omega}, 5\%)|^2$ around the oscillator period discussed above. The reason for this is that the values of $|YR(\omega, \bar{\omega}, 5\%)|^2$ around the oscillator period, and hence $P_e(\bar{\omega}, 5\%)$, vary much more significantly with the oscillator period than $S(\bar{\omega})$ (Fig. 9). $P_e(\bar{\omega}, 5\%)$ is very small relative to $S(\bar{\omega})$ at a very short oscillator period (0.03 s), which can be seen more clearly in Fig. 6, and becomes very large at the period where the FAS is maximum (0.3 s); then $P_e(\bar{\omega}, 5\%)$ decreases relative to $S(\bar{\omega})$ with increasing oscillator period (0.7, 2, 6, and 8 s). Overall, the trend in the relative size of $P_e(\bar{\omega}, 5\%)$ with respect to $S(\bar{\omega})$ with variation of the oscillator period T_0 is consistent with that in the FAS with variation of the period T .

Combining Eq. (17) and the behavior of $|YR(\omega, \bar{\omega}, \xi)|^2$, the trend in the DMF with variation of the oscillator period can then be explained. (1) Since the value of $P_e(\bar{\omega}, 5\%)$ is very small relative to the value of $S(\bar{\omega})$ at very short oscillator periods, values of the DMF at very short oscillator periods are near to the maximum value, i.e., unity. (2) Since the value of $P_e(\bar{\omega}, 5\%)$ is very large relative to the value of $S(\bar{\omega})$ at the period where the FAS is maximum, the value of the DMF approaches its minimum at this period. (3) Since the value of $P_e(\bar{\omega}, 5\%)$ decreases relative to the value of $S(\bar{\omega})$ at long oscillator periods, the value of the DMF increases and approaches unity at long oscillator periods. (4) From the overall perspective, since the trend in the relative size of $P_e(\bar{\omega}, 5\%)$ with respect to $S(\bar{\omega})$ with variation of the oscillator period is consistent with that of the FAS with variation of the period T , and the value of the DMF is inversely proportional to the relative size of $P_e(\bar{\omega}, 5\%)$ with respect to $S(\bar{\omega})$; the trend in the DMF with variation of the oscillator period is opposite to that in the FAS with variation of the period T . Therefore, the overall shapes of the DMF and FAS are almost symmetrical with respect to the period axis.

3.2. Dependence of the DMF on the damping ratio

The dependence of the DMF on the damping ratio is discussed in this section. It can be seen from Fig. 2 (a) that the trend in the DMF with variation of the damping ratio is also typically consistent with that observed from statistical analysis of recorded seismic motions [15,19]. The value of the DMF decreases with increasing damping ratio at all oscillator periods. Fig. 10 shows some representative values of the DMF versus the damping ratio at several oscillator periods. In this figure, k_T is a period ratio defined as T_0/T_p , where T_p represents the period at which the peak of the FAS occurs. The value of T_p depends on the seismological parameters, $T_p = 0.3$ s for the FAS in Fig. 10(a), and $T_p = 0.45$ s for the

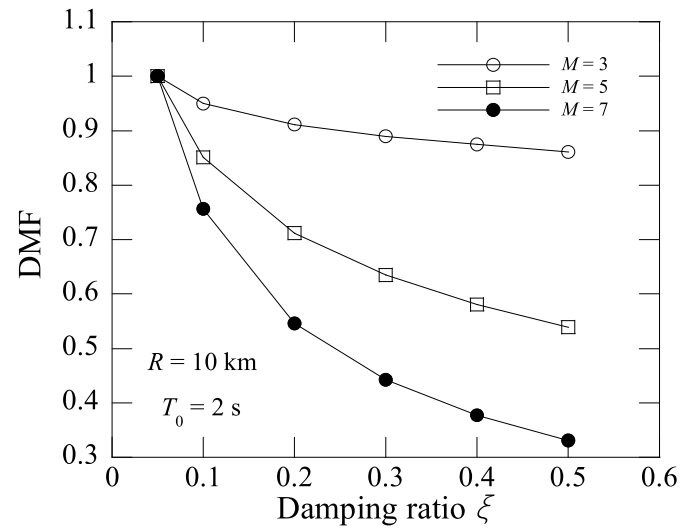


Fig. 11. Influence of magnitude M on the variation of the DMF with the damping ratio ξ .

FAS in Fig. 10(b). Fig. 10 illustrates that the value of the DMF decreases fastest at the period where the FAS is a maximum (or the DMF is a minimum), i.e., $k_T = 1$, with increasing damping ratio. As the period T_0 moves away from T_p , i.e., k_T becomes smaller or larger than unity, the decrease rate of the DMF with increasing damping ratio decreases. The decrease rates for two cases of $k_T < 1$ and $k_T > 1$, may be very close, e.g., $k_T = 0.3$ and 3 in Fig. 10(a).

The trend in the DMF with variation of the damping ratio can be explained by referring Figs. 7 and 8 again. The values of the oscillator transfer function decrease with increasing damping ratio, $|YR(\omega, \bar{\omega}, \xi)|^2$, and hence its area will also decrease with increasing damping ratio. Therefore, the value of the DMF at any oscillator period decreases with increasing damping ratio. The rate of decrease of the DMF with increasing damping ratio can be explained by further combining Eq. (17). This equation indicates that, the rate of decrease of the DMF depends on the relative size of $P_e(\bar{\omega}, 5\%)$ with respect to $S(\bar{\omega})$. When $P_e(\bar{\omega}, 5\%)$ is very small compared to $S(\bar{\omega})$, the rate of decrease approaches that of $S(\bar{\omega})$; conversely, when $P_e(\bar{\omega}, 5\%)$ is very large relative to $S(\bar{\omega})$, the rate of decrease approaches that of $P_e(\bar{\omega}, \xi)$. Since $P_e(\bar{\omega}, \xi)$ decreases with increasing damping ratio, but $S(\bar{\omega})$ remains almost constant with damping ratio, the rate of decrease of $P_e(\bar{\omega}, \xi)$ is clearly faster than that of $S(\bar{\omega})$. Furthermore, since the size of $P_e(\bar{\omega}, 5\%)$ relative to $S(\bar{\omega})$ nearly reaches its maximum at the period where the FAS is maximum, as introduced above, the value of the DMF decreases fastest at this period with increasing damping ratio. As the period T_0 moves away from T_p , i.e., k_T becomes smaller or larger than unity, since $P_e(\bar{\omega}, 5\%)$ decreases relative to $S(\bar{\omega})$ as introduced above, the decrease rate of the DMF with increasing damping ratio decreases.

3.3. Dependence of the DMF on the seismological parameters

The dependence of the DMF on the seismological parameters, including magnitude M , site-to-source distance R , and site conditions, is discussed in this section. Firstly, the dependence of the DMF on the magnitude M is discussed. It is observed from Fig. 2 (b) that the trend in the DMF with variation of the magnitude is typically consistent with the trend observed from statistical analysis of recorded seismic motions [19]. At long oscillator periods, the values of the DMF decrease significantly and become less dependent on the oscillator period with increasing magnitude M . This point can also be known by comparing Fig. 10(a) and (b). In addition, it can be seen by comparing Figs. 1 and 2 (b) that the trend in the DMF with variation of the magnitude M is exactly opposite to that in the FAS; and no matter how the DMF and FAS

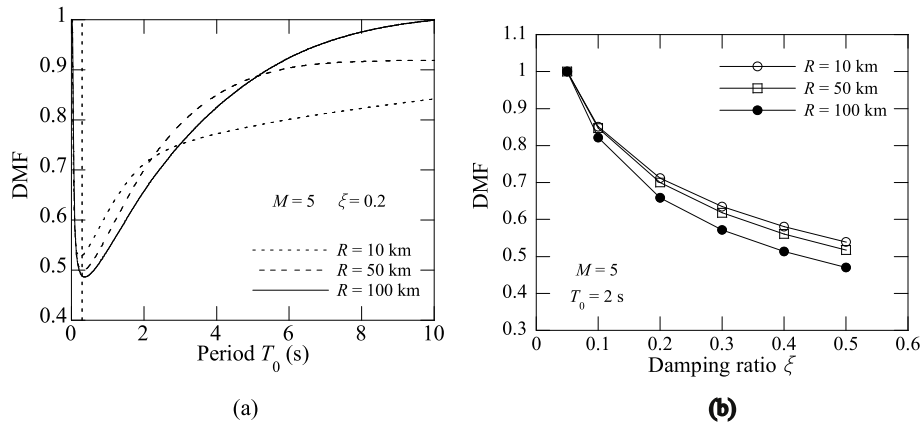


Fig. 12. Influence of the site-to-source distance R on variations of the DMF with the (a) period T_0 ; and (b) damping ratio ξ .

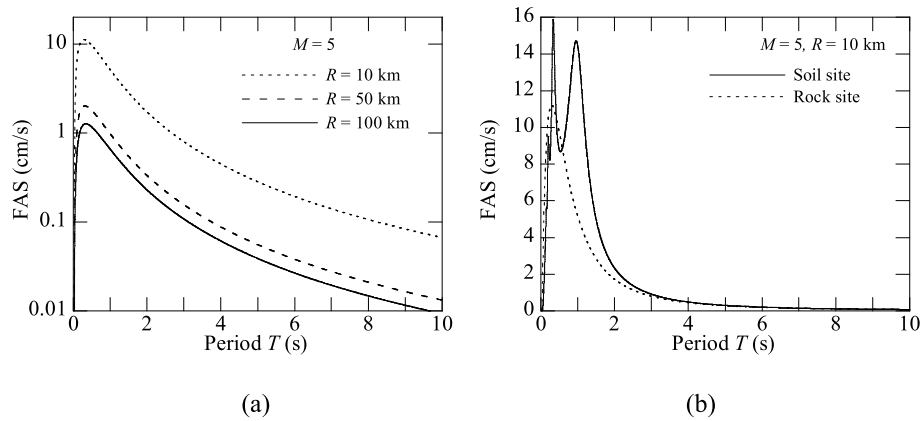


Fig. 13. Comparison of Fourier amplitude spectra with different (a) site-to-source distances and (b) site conditions.

vary with magnitude, their overall shapes retain mutual symmetry with respect to the period axis. Fig. 11 presents some representative values of the DMF versus the damping ratio ξ for the three magnitudes at a long oscillator period. It is found that the decrease rate of the DMF with ξ increases as magnitude M is increased.

To investigate the trend in the DMF with variation of the site-to-source distance R , values of the DMF for three different site-to-source distances ($R = 10, 50, \text{ and } 100 \text{ km}$) are compared in Fig. 12, and the corresponding FAS plots are shown in Fig. 13(a). It is noted that, compared to magnitude M (Figs. 2(b) and 11), the DMF varies much less with the site-to-source distance R , and the variation shows no clearly trend. The trend in the DMF with variation of the site-to-source distance R is also consistent with the trend observed from statistical analysis of recorded seismic motions [19,24].

Furthermore, the trend in the DMF with variation of site conditions is explored. It should be noted that the site term in the FAS model in Section 2.1 corresponds to a generic rock site appropriate for coastal California [35]. To explore effect of site conditions on the DMF, another soil site is considered. The soil site is composed of a single 37.5 m-depth soil layer on a half-space bedrock. The shear-wave velocities of the soil layer and the half-space bedrock are 150 and 750 m/s, respectively. The damping ratios of the soil layer and the half-space bedrock are set as 10% and zero, respectively. Thus, the undamped site fundamental period is 1.0 s, and the impedance ratio of the soil layer with respect to the half-space bedrock is 0.2. The FAS at the soil site can then be obtained from that at the rock site, and the results at the soil and rock sites are compared in Fig. 13(b). Fig. 14 shows the values of the DMF at the rock and soil sites. For the soil site, it is found that the overall shapes of the DMF and FAS are still symmetrical with respect to the period axis,

the valleys of the DMF occur at periods where the peaks of the FAS occur, and the peaks of the DMF occur at periods where the valleys of FAS occur (Fig. 14(a)). The peaks of the FAS at the soil site occur at the resonance periods (1 s and 0.33 s) of the soil site. In addition, comparing the DMF at the rock site with its values at the soil sites, they become smaller at the oscillator periods around the valleys (or the peaks of the FAS) (Fig. 14(a)), and become larger at oscillator periods longer than about 2 s (Fig. 14(a)). The decrease rate of the DMF with ξ becomes faster at the site fundamental period (Fig. 14(b)), and slower at long oscillator periods (Fig. 14(c)).

The variation of the shape of the DMF with the seismological parameters can be explained based on the first term of Eq. (16). It is noted that the variation of the DMF with the magnitude, source-to-site distance, or site conditions is solely due to the change in the FAS, because the other factor affecting the DMF, i.e., the oscillator transfer function, does not change with these seismological parameters. In addition, since the first term of Eq. (16) is expressed in the form of a ratio related to the FAS, it is the relative values (or the shape) of the FAS at different periods instead of its absolute values that really affect the DMF. Thus, when shape of the FAS changes with the magnitude, source-to-site distance, or site conditions, the DMF will change accordingly. It was noted in Section 3.1 that the overall shapes of the DMF and FAS are nearly symmetrical with respect to the period axis. The reason for this is that the trend in the values of $|YR(\omega, \bar{\omega}, 5\%)|^2$ around the oscillator period (or the relative size of $P_e(\bar{\omega}, 5\%)$ with respect to $S(\bar{\omega})$) with variation of the oscillator period is consistent with that in the FAS with variation of the period T . Fig. 15 further shows values of $|YR(\omega, \bar{\omega}, 5\%)|^2$ for a variety of oscillator periods for ground motions with a larger magnitude ($M = 7$) and at the soil site. It is found that, no matter how the FAS changes with the

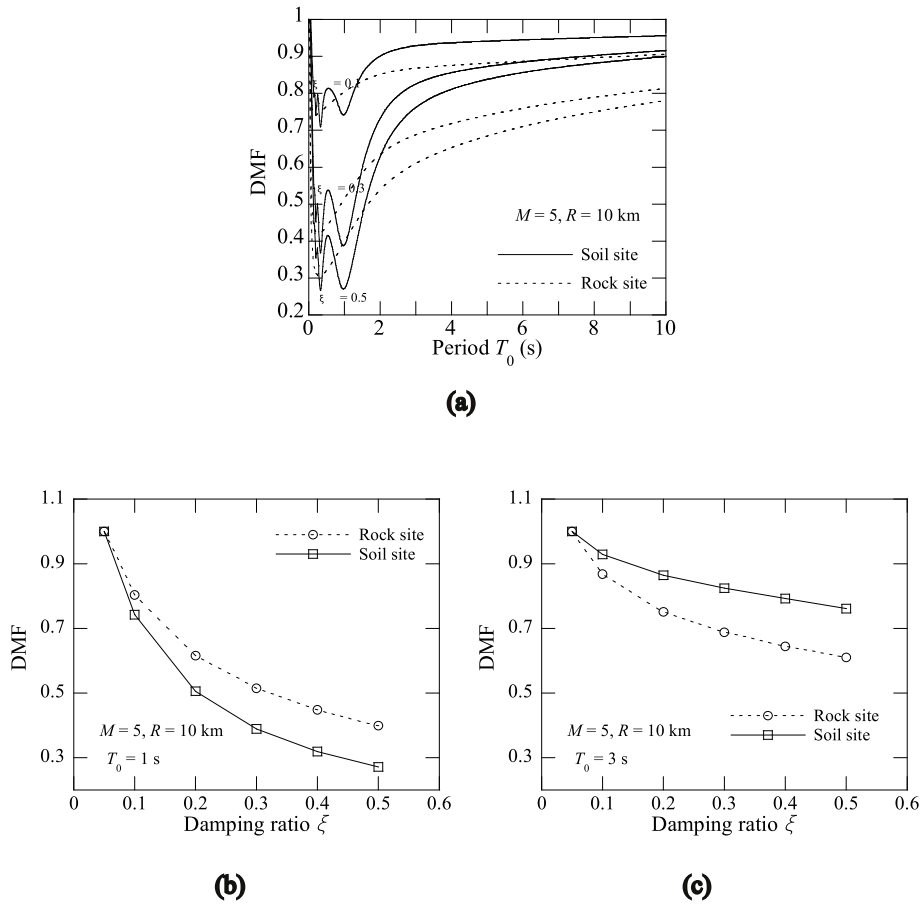


Fig. 14. Influence of site conditions on variations of the DMF with the (a) period T_0 ; (b) damping ratio ξ at the site fundamental period; and (c) damping ratio ξ at long oscillator periods.

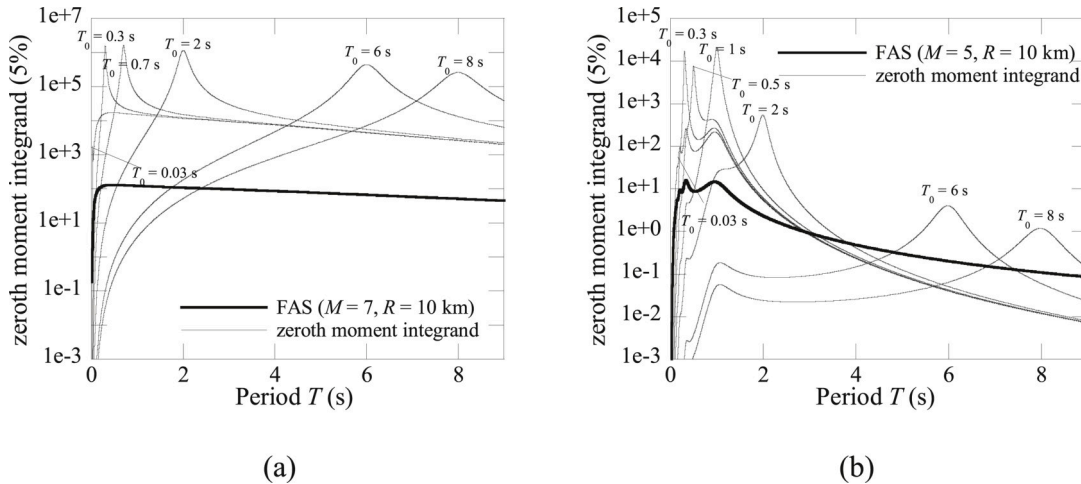


Fig. 15. Variation of $|YR(\omega, \bar{\omega}, 5\%)|^2$ with the oscillator period for (a) ground motion with $M = 7$; (b) ground motion at the soil site.

magnitude or site conditions, the trend in the values of $|YR(\omega, \bar{\omega}, 5\%)|^2$ around the oscillator period (or the relative size of $P_e(\bar{\omega}, 5\%)$ with respect to $S(\bar{\omega})$) with variation of the oscillator period is always consistent with that in the FAS with variation of the period T . This explains why the overall shapes of the DMF and FAS are always symmetrical with respect to the period axis. Therefore, when the long-period component of the FAS increases relatively with increasing magnitude, the values of the DMF at long oscillator periods become less dependent on oscillator period. When the FAS is filtered by the soil site and peaks

appear at the soil resonance periods, valleys appear in the DMF at the corresponding periods; conversely, when valleys appear in the FAS between the soil resonance periods, peaks appear in the DMF. Furthermore, since the FAS does not change significantly in shape with the source-to-site distance (Fig. 13(a)), variation in the DMF with varying source-to-site distance is not obvious and has no regularity.

The behavior of the absolute values of the DMF with variation of the magnitude and site conditions can be explained based on Eq. (17). As introduced above, the value of the DMF is inversely proportional to the

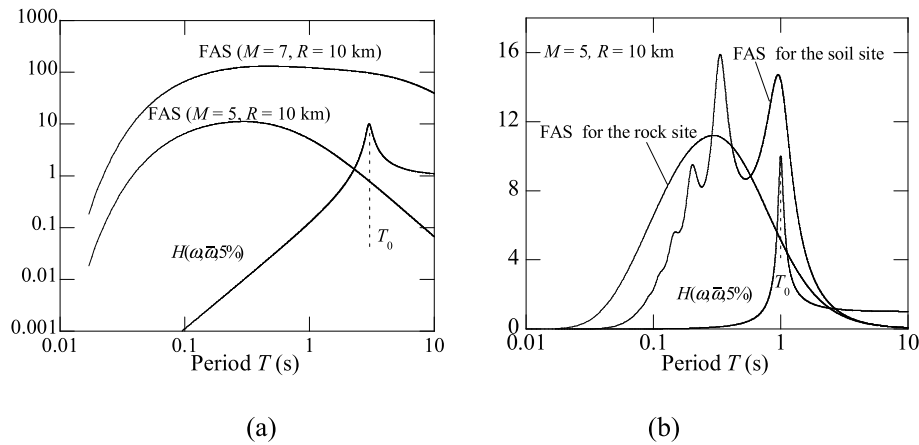


Fig. 16. Illustration of the behavior of the absolute values of the DMF with variation of (a) the magnitude and (b) site conditions.

relative size of $P_e(\bar{\omega}, 5\%)$ with respect to $S(\bar{\omega})$, and both $P_e(\bar{\omega}, 5\%)$ and $S(\bar{\omega})$ change with the FAS. Since the rate of reduction in the area of $|YR(\omega, \bar{\omega}, \xi)|^2$ around the oscillator period with changing damping ratio $r(\xi)$ is mainly affected by the oscillator transfer function, $r(\xi)$ is approximately considered to be independent of the FAS. Fig. 16(a) indicates that, when the long-period components of the FAS increase relatively with increasing magnitude, at long oscillator periods, the rate of increase in values of $|YR(\omega, \bar{\omega}, 5\%)|^2$ at periods around the oscillator period is larger than that of values at short periods; thus, the relative size of $P_e(\bar{\omega}, 5\%)$ with respect to $S(\bar{\omega})$ at long oscillator periods increases with increasing magnitude. Therefore, values of the DMF at long oscillator periods decrease with increasing magnitude. In addition, since the decrease rate of $P_e(\bar{\omega}, \xi)$ with ξ is faster than that of $S(\bar{\omega})$, the decrease rate of the DMF with ξ increases as magnitude M is increased. Similarly, Fig. 16(b) indicates that when the components of the FAS around the soil resonance periods (0.3, and 1.0 s) increase relatively as a result of the ground motion propagating through the soil layer; at oscillator periods equaling the soil resonance periods, the rate of increase in values of $|YR(\omega, \bar{\omega}, 5\%)|^2$ at periods around the oscillator period will be larger than that in the values at other periods. Thus, the relative size of $P_e(\bar{\omega}, 5\%)$ with respect to $S(\bar{\omega})$ at oscillator periods equaling the soil resonance periods increases. Therefore, values of the DMF at oscillator periods equaling the soil resonance periods decrease as a result of the ground motion propagating through the soil layer. And therefore, the decrease rate of the DMF with ξ at the site fundamental period becomes faster (Fig. 14(b)). The increase in the components of the FAS around the soil resonance periods (0.3–2 s) also means a relative decrease in the components at longer period (>2 s), although their absolute values do not change (Fig. 13 (b)). Thus, at longer oscillator periods (>2 s), the rate of increase in the values of $|YR(\omega, \bar{\omega}, 5\%)|^2$ at periods around the oscillator period is smaller than that in the values at short periods (0.3–2 s); thus, the relative size of $P_e(\bar{\omega}, 5\%)$ with respect to $S(\bar{\omega})$ at longer oscillator periods (>2 s) decreases. Therefore, values of the DMF at long oscillator periods (>2 s) increase as a result of the ground motion propagating through the soil layer. And therefore, the decrease rate of the DMF with ξ at long oscillator periods becomes slower (Fig. 14(c)).

4. Conclusions

This study presents a new theoretical approach to analysis of the DMF. The earthquake ground motion is modeled as a source-based FAS that explicitly incorporates various seismological parameters. An equation for estimation of the DMF is derived using the FAS based on RVT. Using the developed approach, trends in the DMF with variation of the structural and seismological parameters are explored and explained in detail. The main findings of this study can be summarized as follows.

- (1) The trend in the DMF with variation of the oscillator period is mainly controlled by the shape of the FAS, and it is opposite to the trend in the FAS with variation of its period. The overall shapes of the DMF and FAS are nearly symmetrical with respect to the period axis. The minimum value of the DMF occurs at nearly the same period as the peak of the FAS.
- (2) The value of the DMF decreases with increasing damping ratio, and the rate of decrease is greatest at the period where the FAS is maximum.
- (3) The trend in the DMF with variation of the seismological parameters is also mainly controlled by the shape of the FAS. When the FAS changes with the seismological parameters, the DMF changes accordingly, and their overall shapes almost always retain symmetry with respect to the period axis. When long-period components of the FAS increase with increasing magnitude, the values of the DMF at long oscillator periods decrease and become less dependent on the oscillator period. When the FAS is filtered by a soil layer, valleys appear in the DMF at periods where the peaks of the FAS occur and peaks appear at periods where the valleys of the FAS occur. Due to there being minimal change in the shape of the FAS when varying the source-to-site distance, the DMF does not change significantly with source-to-site distance.

Declaration of competing interest

None.

CRediT authorship contribution statement

Haizhong Zhang: Conceptualization, Methodology, Writing - original draft, Investigation. **Yan-gang Zhao:** Data curation, Visualization, Supervision, Writing - review & editing.

Acknowledgements

The study is partially supported by the National Natural Science Foundation of China (Grant No. 51738001). The support is gratefully acknowledged.

Appendix A. Supplementary data

Supplementary data to this article can be found online at <https://doi.org/10.1016/j.soildyn.2020.106225>.

References

- [1] Naem F, Kelly JM. Design of seismic isolated structures. From theory to practice. New York: John Wiley and Sons; 1999.
- [2] Constantinou MC, Soong TT, Dargush GF. Passive energy dissipation systems for structural design and retrofit, monograph series. New York: MCEER, Buffalo; 1998.
- [3] Newmark NM, Hall WJ. Earthquake spectra and design EERI monograph series. Oakland, CA: Earth Eng Research Inst; 1982.
- [4] UBC. Uniform building code, international conference of building officials. 1997 [Whittier, CA].
- [5] IBC. International building code. Whittier, CA: International Conference of Building Officials; 2000.
- [6] Kawashima K, Aizawa K. Modification of earthquake response spectra with respect to damping ratio. Proceedings of the 3rd US national conference on earthquake engineering, vol. II. Charleston, SC; 1986. p. 1107–16.
- [7] Caltrans seismic design Criteria 2004, California, Department of Transportation, [Sacramento, California, USA].
- [8] Ashour SA. Elastic seismic response of buildings with supplemental damping. Michigan University: Ph.D. Thesis, Department of Civil Engineering; 1987.
- [9] UBC. Uniform building code, international conference of building officials. 1994 [Whittier, CA].
- [10] Bommer JJ, Elnashai AS. Displacement spectra for seismic design. *J Earthq Eng* 1999;3:1–32.
- [11] Eurocode 8. Design of structures for earthquake resistance, Part 1: general rules, seismic actions and rules for buildings. Brussels: CEN; 2004. EN 2004-1-1.
- [12] Tolis SV, Faccioli E. Displacement design spectra. *J Earthq Eng* 1999;3:107–25.
- [13] Ramirez OM, Constantinou MC, Kircher CA, Whittaker AS, Johnson MW, Gomez JD, Chrysostomou CZ. Development and evaluation of simplified procedures for analysis and design of buildings with passive energy dissipation systems. New York: Multidisciplinary Center for Earthquake Engineering Research (MCEER), University of New York at Buffalo; 2000ReportNo: MCEER-00-0010.
- [14] NEHRP. Recommended Provisions for seismic regulations for new buildings and other structures. Washington DC: Federal Emergency Management Agency; 2000.
- [15] Lin YY, Chang KC. A study on damping reduction factor for buildings under earthquake ground motion. *J Struct Eng* 2003;129:206–14.
- [16] Lin YY, Chang KC. Effects of site classes on damping reduction factors. *J Struct Eng* 2004;130(11):1667–75.
- [17] Bommer JJ, Mendis R. Scaling of spectral displacement ordinates with damping ratios. *Earthq Eng Struct Dynam* 2005;34:145–65.
- [18] Cameron WI, Green RU. Damping correction factors for horizontal ground-motion response spectra. *Bull Seismol Soc Am* 2007;3:934–60.
- [19] Hao A, Zhou D, Li Y, Zhang H. Effects of moment magnitude, site conditions and closest distance on damping modification factors. *Soil Dynam Earthq Eng* 2011;31:1232–47.
- [20] Rezaeian S, Bozorgnia Y, Idriss IM, Abrahamson N, Campbell K, Silva W. Damping scaling factors for elastic response spectra for shallow crustal earthquakes in active tectonic regions: “average” horizontal component. *Earthq Spectra* 2014;30(2):939–63.
- [21] Stafford PJ, Mendis R, Bommer JJ. Dependence of damping correction factors for response spectra on duration and numbers of cycles. *J Struct Eng* 2008;134(8):1364–73.
- [22] Zhou J, Tang K, Wang H, Fang X. Influence of ground motion duration on damping reduction factor. *J Earthq Eng* 2014;18(5):816–30.
- [23] Nagao K, Kanda J. Estimation of damping correction factors using duration defined by standard deviation of phase difference. *Earthq Spectra* 2015;31:761–83.
- [24] Hatzigeorgiou GD. Damping modification factors for SDOF systems subjected to near-fault, far-fault and artificial earthquakes. *Earthq Eng Struct Dynam* 2010;39:1239–58.
- [25] Hubbard DT, Mavroeidis GP. Damping coefficients for near-fault ground motion response spectra. *Soil Dynam Earthq Eng* 2011;31:401–17.
- [26] Khoshnoudian F, Ahmadi E, Azad AI. Damping coefficients for soil–structure systems and evaluation of FEMA440 subjected to pulse-like near-fault earthquakes. *Soil Dynam Earthq Eng* 2014;61–62:124–34.
- [27] Mollaioli F, Liberatore L, Lucchini A. Displacement damping modification factors for pulse-like and ordinary records. *Eng Struct* 2014;78:17–27.
- [28] Pu W, Kasai K, Karoki EK, Huang B. Evaluation of the damping modification factor for structures subjected to near-fault ground motions. *Bull Earthq Eng* 2016;14:1519–44.
- [29] Xiang Y, Huang QL. Damping modification factor for the vertical seismic response spectrum: a study based on Japanese earthquake records. *Eng Struct* 2019;179:493–511.
- [30] Palermo M, Silvestri S, Trombetti T. Stochastic-based damping reduction factors. *Soil Dynam Earthq Eng* 2016;80:168–76.
- [31] Greco R, Fiore A, Marano GC, Briseghella B. Effects of excitation bandwidth on damping reduction factor. *J Earthq Eng* 2018:1–28.
- [32] Greco R, Fiore A, Briseghella B. Influence of soil type on damping reduction factor: a stochastic analysis based on peak theory. *Soil Dynam Earthq Eng* 2018;104:365–8.
- [33] Greco R, Vanzi I, Lavorato D, Briseghella B. Seismic duration effect on damping reduction factor using random vibration theory. *Eng Struct* 2019;179:296–309.
- [34] Clough RW, Penzien J. Dynamics of structures. New York: McGraw-Hill, Inc.; 1977.
- [35] Boore DM. Simulation of ground motion using the stochastic method. *Pure Appl Geophys* 2003;60:635–76.
- [36] Boore DM. Stochastic simulation of high-frequency ground motions based on seismological models of the radiated spectra. *Bull Seismol Soc Am* 1983;73:1865–94.
- [37] Boore DM, Joyner WB. Site amplifications for generic rock sites. *Bull Seismol Soc Am* 1997;87:327–41.
- [38] Atkinson GM, Boore DM. Ground motion relations for eastern North America. *Bull Seismol Soc Am* 1995;85:17–30.
- [39] Frankel A, Mueller C, Barnhard T, Perkins D, Leyendecker E, Dickman N, Hanson S, Hopper M. National seismic hazard maps: documentation June 1996. U.S. Geol. Surv. Open-File Rept. 96–532, 69 pp.
- [40] Hanks TC, McGuire RK. The character of high-frequency strong ground motion. *Bull Seismol Soc Am* 1981;71:2071–95.
- [41] Rathje EM, Ozbey MC. Site-specific validation of random vibration theory-based seismic site response analysis. *J Geotech Geoenviron Eng* 2006;132(7):911–22.
- [42] Kottke AR, Rathje EM. Comparison of time series and random-vibration theory site-response methods. *Bull Seismol Soc Am* 2013;103:2111–27.
- [43] Wang X, Rathje EM. Influence of peak factors on site amplification from random vibration theory based site-response analysis. *Bull Seismol Soc Am* 2016;106:1–14.
- [44] Wang X, Rathje EM. Development of ground-motion duration models for use in random vibration theory site-response analysis. *Bull Seismol Soc Am* 2018;108:2104–16.
- [45] Wang X, Rathje EM. Accounting for changes in duration in random-vibration-theory-based site-response analysis. *Bull Seismol Soc Am*; 108: 2117–2129.
- [46] Cartwright DE, Longuet-Higgins MS. The statistical distribution of the maxima of a random function. *Proc Roy Soc Lond Math Phys Sci* 1956;237:212–23.
- [47] Davenport AG. Note on the distribution of the largest value of a random function with application to gust loading. *Proc Inst Civ Eng* 1964;28:187–96.
- [48] Vanmarcke EH. On the distribution of the first-passage time for normal stationary random processes. *J Appl Mech* 1975;42:215–20.
- [49] Boore DM, Joyner WB. A note on the use of random vibration theory to predict peak amplitudes of transient signals. *Bull Seismol Soc Am* 1984;74:2035–9.
- [50] Liu L, Pezeshk S. An improvement on the estimation of pseudoresponse spectral velocity using RVT method. *Bull Seismol Soc Am* 1999;89:1384–9.
- [51] Atkinson GM, Silva W. Stochastic modeling of California ground motions. *Bull Seismol Soc Am* 2000;90:255–74.
- [52] Boore DM, Thompson EM. Empirical improvements for estimating earthquake response spectra with random-vibration theory. *Bull Seismol Soc Am* 2012;102:761–72.
- [53] Boore DM, Thompson EM. Revisions to some parameters used in stochastic-method simulations of ground motion. *Bull Seismol Soc Am* 2015;105:1029–41.